



Rational design and fabrication of multifunctional catalyst Co₂SnO₄-SnO₂/GC for catalysis applications: Photocatalytic degradation/catalytic reduction of organic pollutants

Jianhua Zheng, Lei Zhang*

College of Chemistry, Liaoning University, 66 Chongshan Middle Road, Shenyang, Liaoning, 110036, People's Republic of China



ARTICLE INFO

Keywords:
Co₂SnO₄-SnO₂/GC
Heterojunctions catalyst
Photocatalytic degradation
Catalytic reduction
Organic contaminant

ABSTRACT

Hollow porous Co₂SnO₄-SnO₂/graphite carbon (Co₂SnO₄-SnO₂/GC) nanocube heterojunction was designed and constructed as advanced catalytic material by calcining CoSn(OH)₆ precursors followed an immersion carbon coating (using the recyclable napkin as graphite carbon source) and calcinations treatment. The design methods focus on forming intimate interfacial contacts among Co₂SnO₄, SnO₂ and GC (*in situ* hybridization of the composite). The obtained Co₂SnO₄-SnO₂/GC exhibits remarkable dual catalytic behavior including the high catalytic efficiency for photocatalytic (under visible light) degradation of chlorotetracycline (CTC)/tetracycline (TC) and catalytic reduction of *p*-nitrophenol (*p*-NP). Co₂SnO₄-SnO₂/GC could be recycled more than four times, preserving its activity and stability based on graphite carbon protective layer on the surface of catalysts. Owing to multiple heterojunctions structure features and the synergistic effects of different junctions, greatly enhance the charge carrier generation and suppress the charge recombination of electron-hole pairs, which would be beneficial to improve its catalytic activity. The possible mechanisms for the dual-functional catalytic reactions for organic contaminants over Co₂SnO₄-SnO₂/GC were made a thorough inquiry. This study not only shows a possibility for the utilization of low cost the recyclable napkin as a substitute for graphene but also provides a new insight into the design and construction of new heterojunction catalysts for enhancing catalytic activity.

1. Introduction

Antimicrobial agents released in the environment such as chlorotetracycline (CTC) and tetracycline (TC), are more difficult to be degraded by bio-treatment and common physicochemical methods because of theirs high chemical stability, which can seriously pose a threat to most of living organisms. Moreover, *p*-nitrophenol (*p*-NP) is one of most notorious industrial organic contaminants possessing carcinogenic character and high toxicity. At present, most of the antimicrobial agents and nitrophenol have been listed as priority pollutants [1,2]. It is no doubts that decomposing contaminants to nontoxic species or transforms to reusable compounds will be a satisfying strategy of remediation for such contaminants. One effective way to solve this problem is to develop multifunctional catalysts with high catalytic activity. Thus, the search for novel catalytic materials for decomposing (effectively transforms) pollutants to nontoxic (reusable) species is urgently needed [3–5].

Stannate bimetal oxides like Zn₂SnO₄ [6–10], BaSnO₃ [11–15], Cd₂SnO₄ [16], and Co₂SnO₄ [17], have been widely studied and developed for various applications such as solar cells, gas sensors, Li-ion

batteries, photocatalysts, due to their high theoretical capacity, low cost and ease of availability. So far, composite heterostructures of stannate bimetal oxides including Ag@AgCl/Zn₂SnO₄ [18], Zn₂SnO₄/grapheme [19], Zn₂SnO₄/ZnO [20], Zn₂SnO₄-carbon [21], Mn₃O₄/Zn₂SnO₄ [22], Co₂SnO₄-multiwalled carbon [23], CoSnO₃@Co₃O₄ [24], and CoSnO₃@C [25], have been reported to show a superior photoelectric behavior compared to pure stannate-based bimetal oxides. However, above-mentioned composites were usually constructed through multiple steps by separately preparing the different materials and then blending them by coating route. Development of a facile and environmentally friendly method for incorporating the different components into a composite would be greatly beneficial for enhancing photoelectric performances of heterostructures materials. Among the Stannate-based bimetal oxides, spinel Co₂SnO₄ has been proven to be a highly promising performers for its small band gap and high electron mobility [26,27]. To date, there are very few reports on the photo-degradation and the catalytic reduction of contaminants using Co₂SnO₄ composites as multifunctional catalysts.

In this paper, an effective strategy has been proposed to papered 3D hollow Co₂SnO₄-SnO₂/GC nanocube by a facile, inexpensive, relative

* Corresponding author.

E-mail address: zhanglei63@126.com (L. Zhang).

green and eco-friendly synthetic route. In particular, in situ growth SnO_2 and Co_2SnO_4 can well incorporate each other and create the intimate contact in the heterojunction region, assuring rapid migration of electrons from the Co_2SnO_4 to SnO_2 , which can greatly accelerate carriers transfer and improve charge separation efficiency [28]. The obtained $\text{Co}_2\text{SnO}_4\text{-SnO}_2/\text{GC}$ exhibited superior catalytic performance and the excellent stability.

2. Experiment section

2.1. Materials

$\text{SnCl}_4\cdot 5\text{H}_2\text{O}$, $\text{CoCl}_2\cdot 6\text{H}_2\text{O}$, and NaOH are of analytical grade and were obtained from Sinopharm Chemical Reagent Co., Ltd. (China). Chlorotetracycline (CTC), Tetracycline (TC) and *p*-nitrophenol (*p*-NP) were purchased from Shanghai Shunbo Biological Engineering Co. Ltd. whereas the napkin was collected from the local restaurants.

2.2. Preparation of various catalysts

2.2.1. Synthesis of hollow CoSnO_3 nanocube

In a typical synthesis, 15 mL of ethanol solution of $\text{SnCl}_4\cdot 6\text{H}_2\text{O}$ (3 mmol) was added to the mixture dissolving $\text{CoCl}_2\cdot 6\text{H}_2\text{O}$ (3 mmol) and $\text{C}_6\text{H}_5\text{Na}_3\text{O}_7\cdot 2\text{H}_2\text{O}$ (3 mmol) under stirring. Consecutively, 15 mL 2.0 mol L^{-1} NaOH was added drop by drop to the mixture under stirring. After 1.5 h, 60 mL 8.0 mol L^{-1} NaOH was added gradually into above mixture. The obtained precipitant was rinse-centrifugation with deionized water and ethanol for several times until to remove excess NaOH and then annealed in N_2 flow at 500 °C for 2 h with a slow ramp rate of 2 °C min^{-1} .

2.2.2. Synthesis of $\text{Co}_2\text{SnO}_4\text{-SnO}_2/\text{GC}$

Firstly, the napkin was cleaned with by immersion in a mixture of ethanol and deionized water (1:1, v/v) for 12 h and dried at 80 °C. Secondly, the cleaned napkin was immersed in deionized water with stirring vigorously to obtain pulp and then dried at 105 °C. Afterwards, 0.50 g as-prepared CoSnO_3 was dispersed in 30 mL deionized water containing 0.05 g as-prepared pulp, sonicated for 60 min and magnetic stirred for 12 h under ambient conditions to form a homogeneous solution and then the water was evaporated. The pulp will spontaneously coat on the CoSnO_3 NPs and the obtained product was dried at 100 °C over night. Finally, the sample was carbonized in N_2 flow at 600 °C for 3 h. $\text{Co}_2\text{SnO}_4\text{-SnO}_2$ was fabricated without adding napkin using the same process. The process of fabrication is illustrated in the Scheme 1. Additionally, the pure Co_2SnO_4 and SnO_2 were obtained by simple co-

precipitation method according to literatures [29,30].

2.3. Characterization

The powder X-ray diffraction with Cu K α radiation (XRD, D/max-2200, Rigaku, Japan) was used to determine the crystal structure and purity of samples. Raman spectra were performed using Laser Confocal Micro-Raman Spectroscope (LabRAM Aramis). BET specific surface area and N_2 adsorption-desorption isotherms of samples were measured at 77 K using a surface area analyzer (BET Autosorb-iQ, American). Morphology of the samples was characterized by a field emission scanning electron microscope (SEM, S4800, Hitachi Co., Japan). TEM was taken on a transmission electron microscope (TEM, 2100F, JEOL Co., Japan). X-ray photoelectron spectroscopic (XPS) measurement was performed on a Thermo Electron Corporation ESCALAB 250 Xi. UV-vis diffuse reflectance spectra (DRS) were performed with an UV-vis spectrophotometer (Shimadzu, UV-2600 Japan) equipped with an integrating sphere diffuse reflectance accessory.

2.4. Catalytic activities

2.4.1. Photocatalytic activities test

The typical antibiotic CTC/TC was used to evaluate the photocatalytic activities. Typically, the as-prepared catalyst (40 mg) was dispersed in 10 mg L^{-1} of CTC/TC aqueous solution (100 mL). Then the suspension was magnetically stirred for 60 min in the dark to obtain adsorption-desorption equilibrium. Subsequently, the suspension of catalyst and CTC/TC was irradiated by a 500 W xenon lamp with a 420 nm cutoff filter. During the process, about 3 mL suspension was collected at an interval of 20 min and centrifugalizes to remove the catalyst. The concentration of CTC/TC was recorded by the UV-vis spectrophotometer.

2.4.2. Free radical trapping tests

The process is the same as photocatalytic activity test mentioned above except adding corresponding scavengers. Experimentally, 0.5 mM sodium oxalate ($\text{Na}_2\text{C}_2\text{O}_4$, h^+), and 5 mM *tert*-Butanol (T-BuOH, $\cdot\text{OH}$) were utilized for scavengers [31,32]. The addition of N_2/O_2 was bubbled to clarify whether generation of $\cdot\text{O}_2^-$ ($\text{e}^- + \text{O}_2 \rightarrow \cdot\text{O}_2^-$) [33] in the photocatalytic reaction.

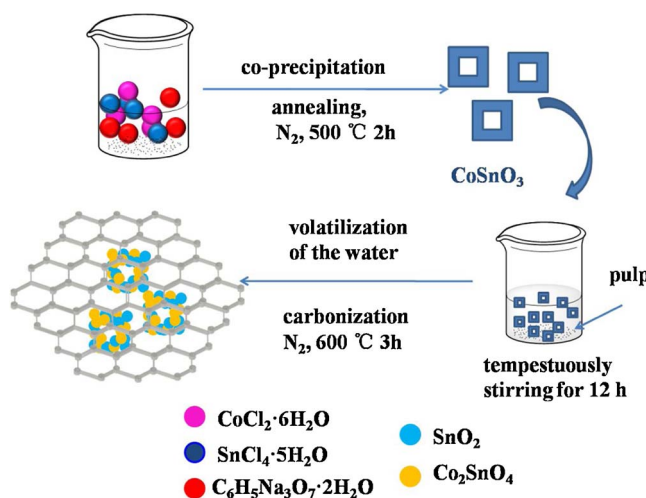
2.4.3. Catalytic reduction test

Typically, 10 mg L^{-1} of *p*-NP aqueous solution (50 mL) and 2 mL of freshly prepared aqueous NaBH_4 (0.1 mol L^{-1}) were successively added into a 100 mL beaker, and then 20 mg catalyst was added into reaction system with stirring constantly. The concentration of *p*-NP was measured by the UV-vis spectrophotometer.

3. Results and discussion

3.1. Catalyst characterization

Scanning electron microscopy (SEM) and transmission electron microscopy (TEM) were applied to confirm the morphology and detailed structure of the as-obtained products. The pure CoSnO_3 displays well-defined nanocube morphologies with a diameter of ca. 200–220 nm (Fig. 1a). As shown in TEM image, the feature of hollow for the nanocube can be clearly observed (inset of Fig. 1a). The cube-shell thickness of CoSnO_3 is about 50 nm. The $\text{Co}_2\text{SnO}_4\text{-SnO}_2$ was obtained after annealing the CoSnO_3 at 600 °C. As Fig. 1b exhibited, $\text{Co}_2\text{SnO}_4\text{-SnO}_2$ well reserves the nanocube shape with an average diameter of ca. 240 nm. The surface of $\text{Co}_2\text{SnO}_4\text{-SnO}_2$ becomes rougher comparing with that of CoSnO_3 . The TEM image confirms that the cavity dimension becomes smaller, exhibiting the general appearance of hierarchical porous (inset of Fig. 1b). The changes can be attributed to the phase change from CoSnO_3 to mixed Co_2SnO_4 and SnO_2 hybrid.



Scheme 1. Schematic illustration of the preparation process of $\text{Co}_2\text{SnO}_4\text{-SnO}_2/\text{GC}$.

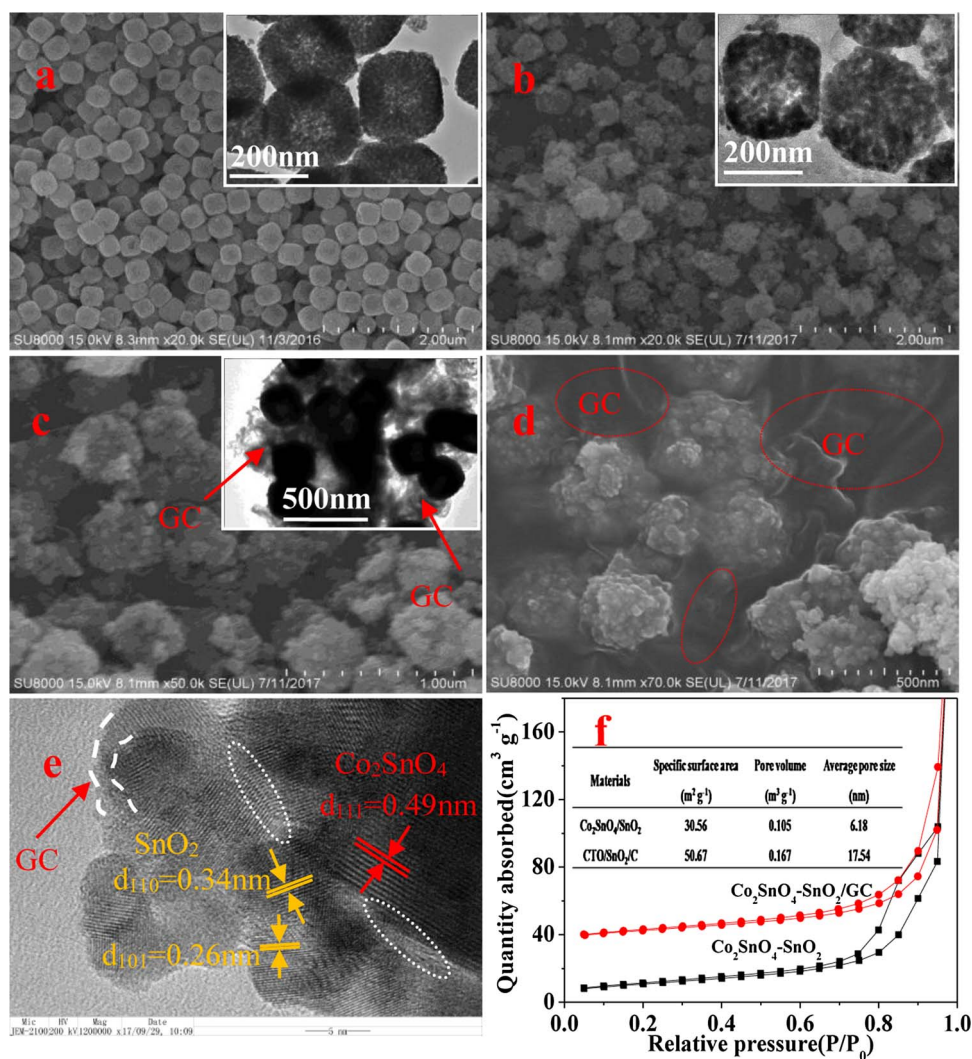


Fig. 1. (a–c) SEM images of CoSnO_3 , $\text{Co}_2\text{SnO}_4\text{-SnO}_2$ and $\text{Co}_2\text{SnO}_4\text{-SnO}_2/\text{GC}$, respectively (d) high-magnification SEM images (e) TEM image and (f) HRTEM image of $\text{Co}_2\text{SnO}_4\text{-SnO}_2/\text{GC}$ composite. Inset: TEM of (a) CoSnO_3 , (b) $\text{Co}_2\text{SnO}_4\text{-SnO}_2$ and (c) $\text{Co}_2\text{SnO}_4\text{-SnO}_2/\text{GC}$, respectively. (For interpretation of the references to colour in the text, the reader is referred to the web version of this article.)

Fig. 1c is the typical SEM image of $\text{Co}_2\text{SnO}_4\text{-SnO}_2/\text{GC}$ hybrid, it can be seen that the $\text{Co}_2\text{SnO}_4\text{-SnO}_2$ nanocube is homogeneously encapsulated by carbon layer (magnified image **Fig. 1d**, indicated by the red circles) with an average diameter of about 260 nm. As the TEM image displayed (inset of **Fig. 1c**), the hollow porous structure is maintained well without noticeable change. The $\text{Co}_2\text{SnO}_4\text{-SnO}_2$ is tightly coated with flake-like GC, revealing to form the $\text{Co}_2\text{SnO}_4\text{-SnO}_2/\text{GC}$ ternary heterojunction hybrid. To further elucidate the nanostructure of $\text{Co}_2\text{SnO}_4\text{-SnO}_2/\text{GC}$, the HRTEM analysis has been performed. The lattice fringes with different distances can be observed in (**Fig. 1e**). The interplanar spacing of 0.49 nm corresponds to (111) lattice planes of Co_2SnO_4 . Analogously, the interplanar distances of lattice fringes calculated to be 0.34 nm and 0.26 nm are attributable to (110) and (101) planes of SnO_2 , respectively. Moreover, some intersections of the lattice fringes can be found in **Fig. 1e** (indicated by the circles), further implying that an intimate contact is formed between SnO_2 and Co_2SnO_4 .

The surface areas and pore structures of $\text{Co}_2\text{SnO}_4\text{-SnO}_2$ and $\text{Co}_2\text{SnO}_4\text{-SnO}_2/\text{GC}$ were characterized by N_2 adsorption-desorption isotherms. Both samples are of type IV (**Fig. 1f**), suggesting the existence of mesoporous in the samples. The specific surface area and cumulative pore volume of samples are listed in inset of **Fig. 1f**. Clearly, the BET of $\text{Co}_2\text{SnO}_4\text{-SnO}_2/\text{GC}$ ($50.67 \text{ m}^2 \text{ g}^{-1}$) is larger than that corresponding value for $\text{Co}_2\text{SnO}_4\text{-SnO}_2$ ($30.56 \text{ m}^2 \text{ g}^{-1}$). The large BET surface area with more active sites is possible to enhancement of the

catalytic activity [34].

The powder X-ray diffraction (XRD) was carried out to insight the crystallinity and phase information of as-obtained $\text{Co}_2\text{SnO}_4\text{-SnO}_2$ and $\text{Co}_2\text{SnO}_4\text{-SnO}_2/\text{GC}$ composite, as displayed in **Fig. 2a**. The characteristic diffraction peaks located at 17.78 (111), 29.20 (220), 34.40 (311), 35.99 (222), 41.79 (400), 55.22 (511), 60.59 (440), and 71.58 (533), which are assigned to Co_2SnO_4 (JCPDS No. 29-0514) [35]. The main diffraction peaks observed at 2 θ values of 26.61 (110), 33.89 (101), 37.95 (200), 51.78 (211), 54.76 (220), 61.87 (310), 64.72 (112) and 65.94 (301) can be easily indexed to SnO_2 (JCPDS No. 41-1445) [36]. In addition, there is no other diffraction peaks corresponding to the low-valence ions (Sn_2O_3) [37]. The CoSn(OH)_6 is thermodynamically unstable. Thus, CoSnO_3 is obtained by thermal-induced dehydration of CoSn(OH)_6 ($\text{CoSn(OH)}_6 \rightarrow \text{CoSnO}_3 + 3\text{H}_2\text{O}$) during the annealed process. After carbon source is introduced, $\text{Co}_2\text{SnO}_4\text{-SnO}_2/\text{GC}$ hybrid was obtained after annealing in N_2 at 600 °C. The synthetic method can cause Co_2SnO_4 and SnO_2 to hybridize in situ ($2\text{CoSnO}_3 \rightarrow \text{Co}_2\text{SnO}_4 + \text{SnO}_2$). Notably, after introduction of carbon, new characteristic diffraction peaks appeared at about 26.60° (inset of **Fig. 2a**), 44.67° and 50.82° in the XRD pattern of $\text{Co}_2\text{SnO}_4\text{-SnO}_2/\text{GC}$, which are well indexed to the (002), (101) and (102) peaks of graphite carbon (JCPDS No. 99-0057) [38]. The results of XRD are consistent with HRTEM patterns.

To further confirm the presence of graphitic carbon, the final

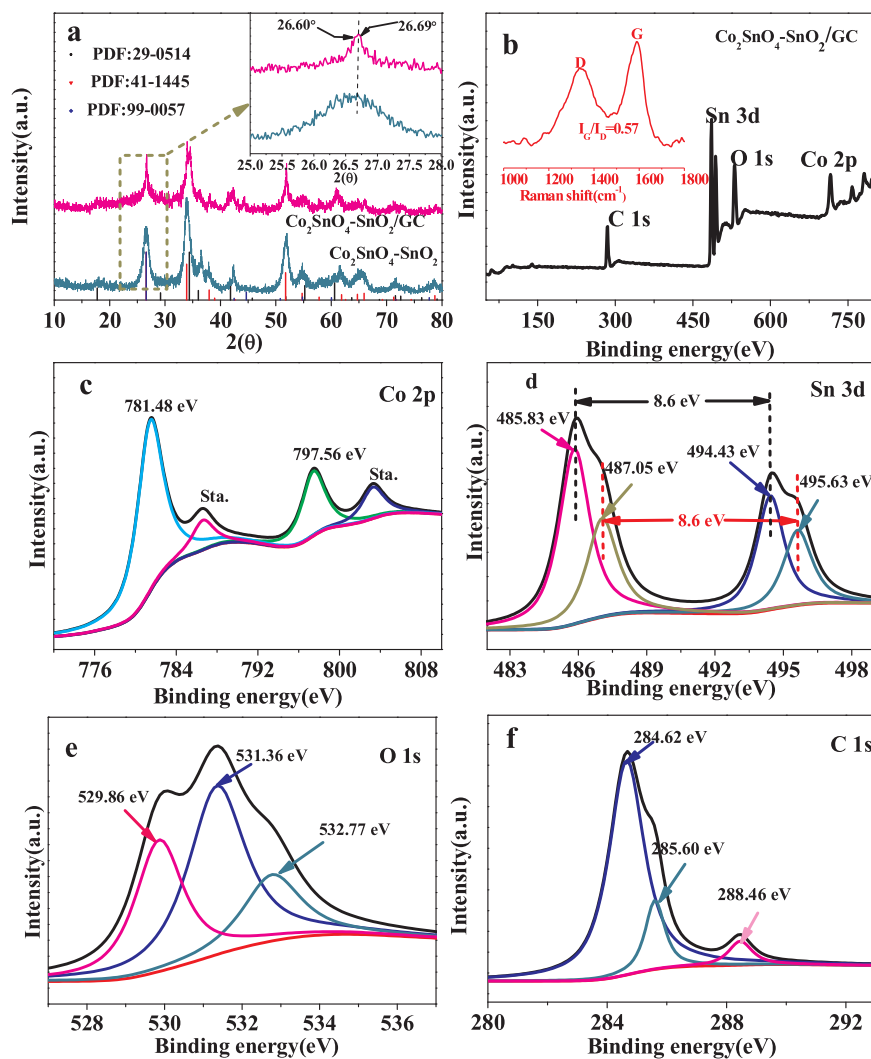


Fig. 2. (a) XRD patterns of samples, (b) XPS of Co₂SnO₄-SnO₂/GC, (c) Co-2p, (d) Sn-3d, (e) O-1s and (f) C-1s, respectively. Inset of (b) Raman spectra of Co₂SnO₄-SnO₂/GC.

Co₂SnO₄-SnO₂/GC products was investigate using Raman spectrum (inset of Fig. 2b). Two main peaks are observed at 1582.63 (G-band) and 1344.58(D-band) cm⁻¹ and the intensity ratio of the G band to the D band (I_G/I_D) was calculated as 0.57, demonstrating the existence of graphite sp² carbon and disordered sp³ carbon, respectively [39].

X-ray photoelectron spectroscopy (XPS) was carried out to confirm the valent state of elements in Co₂SnO₄-SnO₂/GC. The survey XPS spectrum suggests the predominant presence of Co, Sn, O, and C elements, and no other heteroelements were detected (Fig. 2b). The high-resolution XPS spectrum of Co is shown in Fig. 2c. The peaks of Co 2p_{3/2}, Co 2p_{1/2} orbital of diatomic cobalt ions are observed at 781.48 and 797.56 eV with the shake-up satellite (denoted as Sta.) structure at 786.51 and 803.25 [40]. As Fig. 2d shown, the Sn 3d region exhibits two main characteristic peaks, which can be further deconvoluted into two sets of peaks with a spin-orbit splitting energy of ca. 8.6 eV. The peaks separation value corresponds to a binding energy of Sn⁴⁺ [41–43], the peaks centered at 495.63 and 487.05 eV can be ascribed to Sn⁴⁺ of SnO₂ [44]; while the others two peaks denoted as 494.43 and 485.83 eV are attributed to Sn⁴⁺ of Co₂SnO₄, respectively [17,45]. No peaks centered at 494.9 and 486.4 eV with a spin-orbit splitting energy of ca. 8.5 eV was observed, indicating the absence of the chemical state of Sn²⁺ (Sn₂O₃) in Co₂SnO₄-SnO₂/GC hybrid [37]. The O1s spectrum (Fig. 2e) shows three oxygen contributions (529.86 eV, 531.36 and 532.77). The two peaks at 529.86 and 531.36 eV attribute to metal-oxygen bonds (Co-O and Sn-O), while another peak at 532.77

corresponds to -OH [46]. In addition, no peak located at 531.2 eV was observed, which is assigned to the oxygen vacancies [47–49], implying no oxygen vacancies formation under N₂ atmosphere in 600 °C. It is further demonstrate that SnO₂ and Co₂SnO₄ are coexistence in the hybrid system, which is well consist with the XRD analysis. In Fig. 2f, we can find three peaks with the binding energies of 284.62, 285.60 and 288.46, which correspond to reference C-C, C-O and O=C-OH, respectively [50]. The XPS results confirm the successful synthesis of Co₂SnO₄-SnO₂/GC hybrid system.

A serious of experiment including electrochemical impedance spectroscopy (EIS), and photoelectrochemical measurements were carried out to further clarify the hybrid system could enhance the charge transfer and inhibit the recombination of charge-pairs. A smaller diameter indicates a better electronic conductivity and charge transfer performance [51]. Fig. 3a displays EIS Nyquist plots of SnO₂, Co₂SnO₄, Co₂SnO₄-SnO₂, and Co₂SnO₄-SnO₂/GC. It is found that the Co₂SnO₄-SnO₂/GC has a smaller semicircle diameter comparing with SnO₂, Co₂SnO₄ and Co₂SnO₄-SnO₂. The lowest electron transfer resistance attribute to existence heterojunction of Co₂SnO₄, SnO₂ and GC, which helps to improve the efficiency of e⁻/h⁺ pair's separation, making it as a promising catalytic material [52]. The transient photocurrent responses of samples were recorded for four on-off cycles under visible-light irradiation (Fig. 3b). Enhanced photocurrent intensity is observed for Co₂SnO₄-SnO₂/GC compared to Co₂SnO₄-SnO₂, indicating the synergistic effects of Co₂SnO₄-SnO₂ and carbon layer in the hybrid system

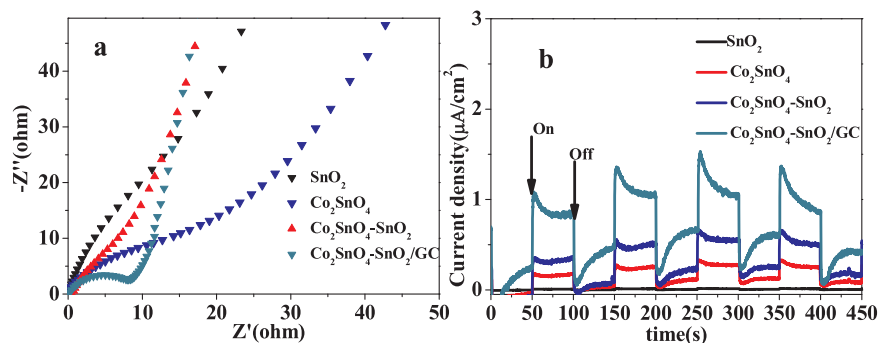


Fig. 3. (a) EIS Nyquist plots at 0.1 V bias potential vs. Ag/AgCl and (b) the periodic on/off photocurrent response at 0.2 V bias potential vs. Ag/AgCl of different samples. (0.1 mol L⁻¹ Na₂SO₄ aqueous solution under visible-light irradiation).

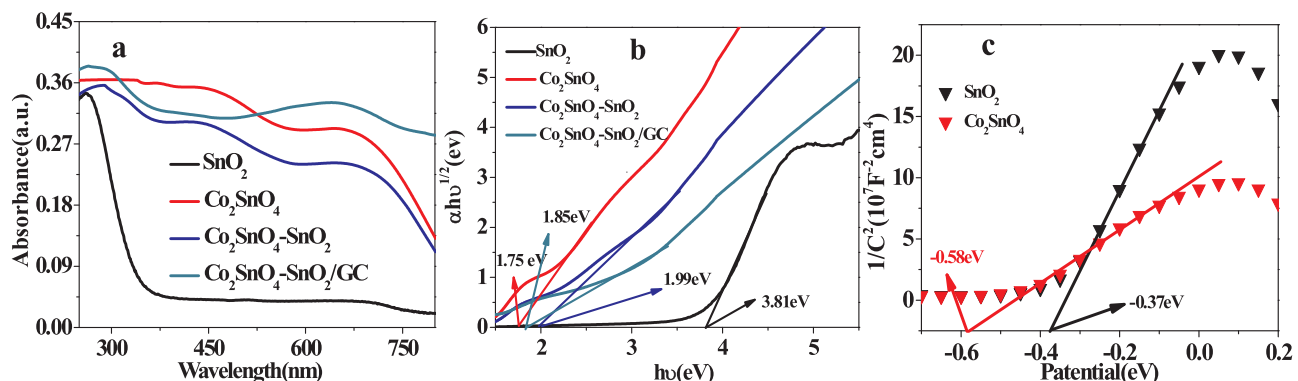


Fig. 4. (a) UV-vis diffuse reflectance spectra of samples (b) their corresponding plots of $(ahv)^{1/2}$ vs. photon energy and (c) the Mott-Schottky plots.

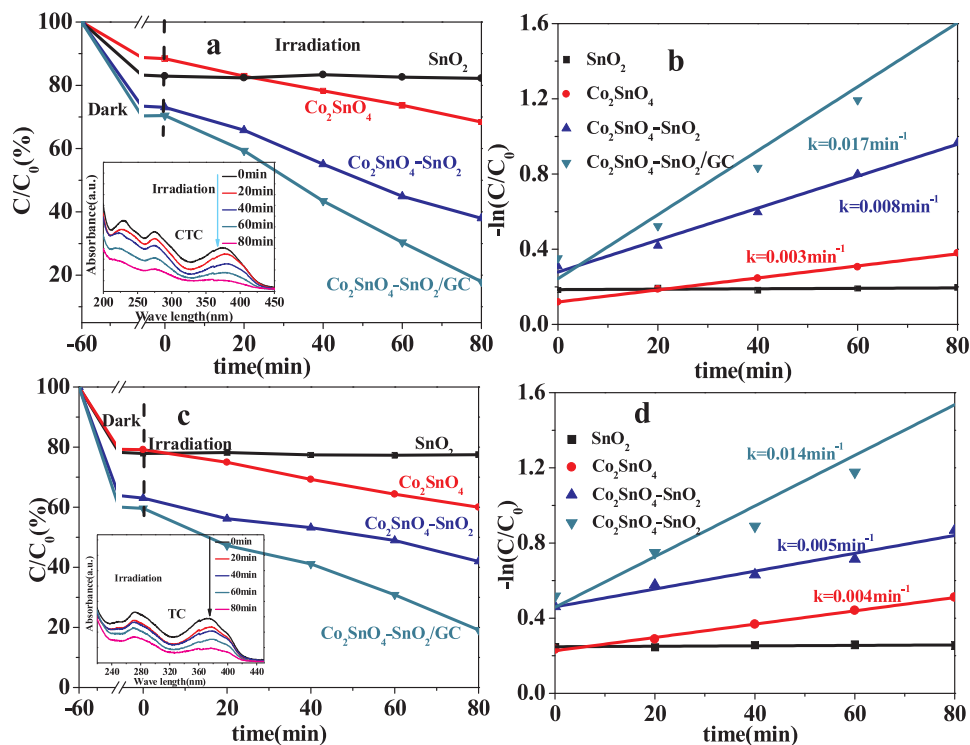


Fig. 5. (a) Photocatalytic degradation of CTC of different samples under visible-light irradiation, (b) the corresponding first-order plots, (c) photocatalytic degradation of TC under visible-light irradiation, and (d) the corresponding first-order plots over different samples.

achieved more efficiently inhibits the recombination of charge-pairs and accelerates rapid charge transfer through $\text{Co}_2\text{SnO}_4\text{-SnO}_2/\text{GC}$ heterojunction [53,54].

Fig. 4a shows UV-vis diffuse reflectance spectra of SnO_2 , Co_2SnO_4 ,

$\text{Co}_2\text{SnO}_4\text{-SnO}_2$, and $\text{Co}_2\text{SnO}_4\text{-SnO}_2/\text{GC}$. It is clear from UV-vis DRS that $\text{Co}_2\text{SnO}_4\text{-SnO}_2/\text{GC}$ hybrid exhibits higher light absorption property under visible light range, due to the interaction between $\text{Co}_2\text{SnO}_4\text{-SnO}_2$ and graphite carbon in the composites. The enhanced light harvesting

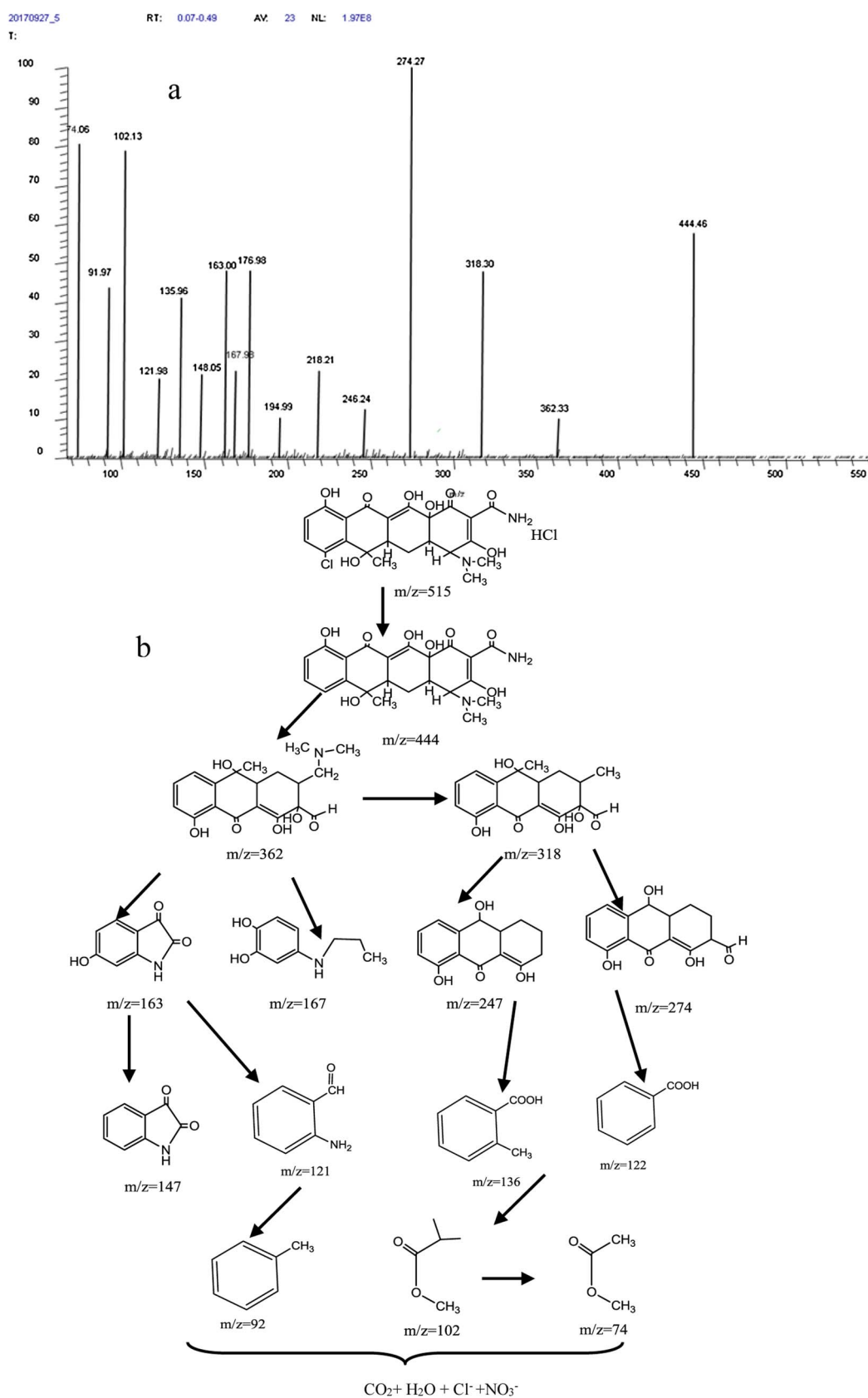


Fig. 6. (a) m/z of the degraded CTC and (b) the proposed main intermediates of the photodegradation of CTC, irradiation by visible light for 80 min.

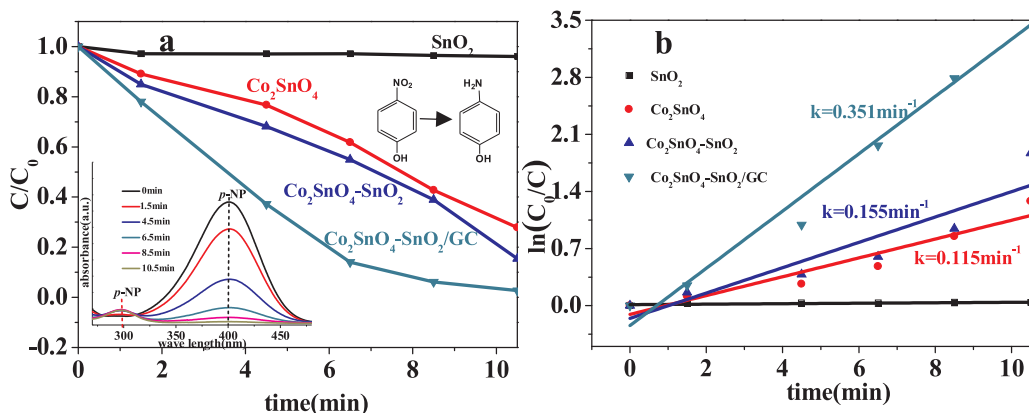


Fig. 7. (a) Catalytic reduction *p*-nitrophenol and (b) the kinetics plots of *p*-nitrophenol reduction over different samples (20 mg catalysts, 50 mL *p*-NP 10 mg L⁻¹).

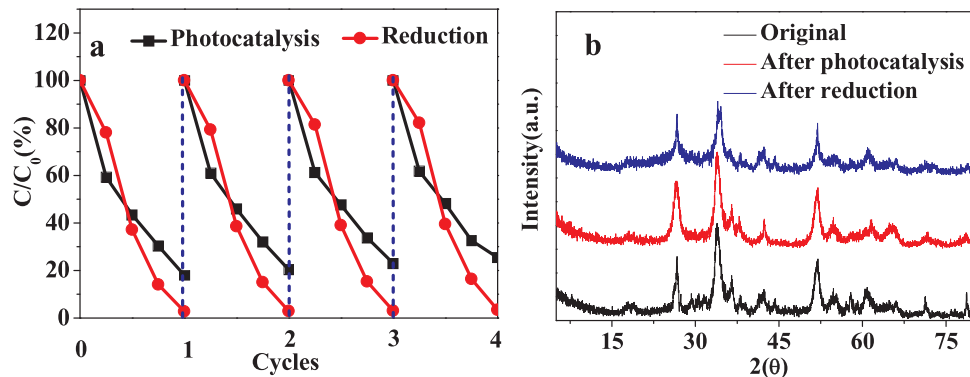


Fig. 8. (a) Cycling experiments for the different reactions by the prepared Co₂SnO₄-SnO₂/GC, and (b) The XRD patterns of Co₂SnO₄-SnO₂/GC before and after cyclic test.

implies that the hybrid catalyst could utilize more visible light. The derived band gaps can be obtained by the Kubelka-Munk theorem (Fig. 4b). The obtained corresponding band gap values for samples are 3.81 eV (SnO₂), 1.75 eV (Co₂SnO₄), 1.99 eV (Co₂SnO₄-SnO₂), and 1.85 eV (Co₂SnO₄-SnO₂/GC). The Mott-Schottky (M-S) method is employed to elucidate the band energy potentials. As the Fig. 4c shown, the flat band potential (E_{FB}) potentials of Co₂SnO₄ and SnO₂ could be confirmed to be -0.58 (-0.34 eV vs. NHE) and -0.37 eV (-0.13 eV vs. NHE), respectively. SnO₂ and Co₂SnO₄ are n-type semiconductors owing to the positive slope of $1/C^2$ versus potential curve, with the conduction band (E_{CB}) position 0.1–0.3 eV higher than that of E_{FB} [55,56]. Herein, the E_{CB} of Co₂SnO₄ and SnO₂ were determined to be -0.44 and -0.23 eV, respectively. Moreover, the valence band (E_{VB}) can be obtained by the formula $E_{VB} = E_{CB} + E_g$. Therefore, the corresponding E_{VB} of Co₂SnO₄ and SnO₂ will occur at about 1.31 and 3.58 eV, respectively.

3.2. Activity measurements of Co₂SnO₄-SnO₂/GC

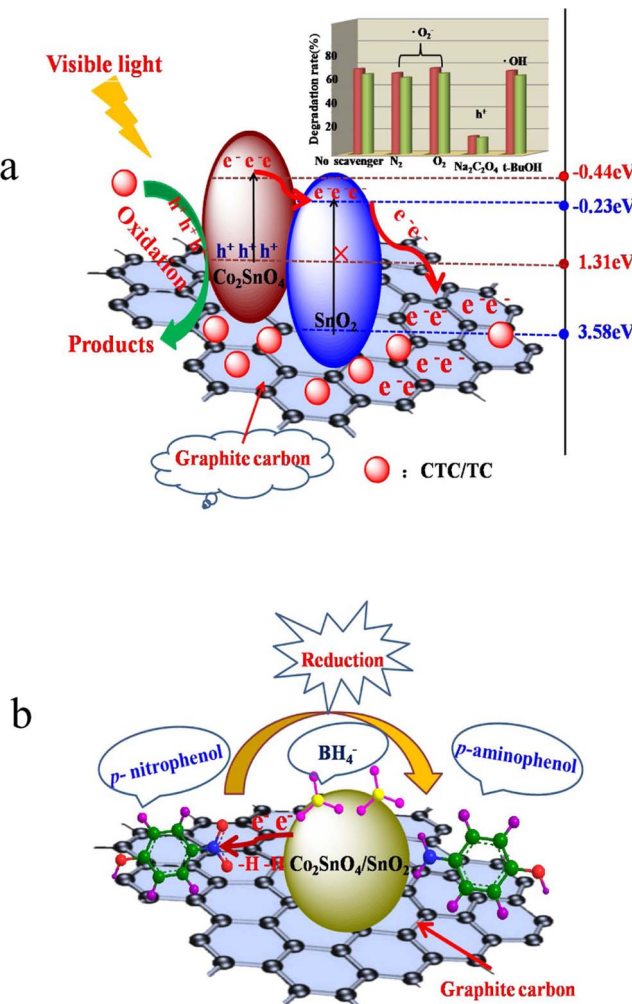
3.2.1. Photocatalytic activity

The photocatalytic performance of Co₂SnO₄-SnO₂/GC hybrid was evaluated by degradation of CTC under visible light irradiation. The degree of the photocatalysis is presented by the ratio of the concentration C/C₀ under various times. Fig. 5a exhibits diagram of the degradation of CTC using different catalysts. Obviously, direct decomposing of CTC under visible light irradiation could be neglected over SnO₂, owing to its lack of response to visible light. It can be clearly observed that pure Co₂SnO₄ and Co₂SnO₄-SnO₂ decomposed 32% and 63% TCT, respectively; while the removal efficiency of CTC reaches to about 83% over Co₂SnO₄-SnO₂/GC.

The inset of Fig. 5a shows the changes of absorbance of CTC over Co₂SnO₄-SnO₂/GC. Clearly, the intensity of the characteristic peak

decreases with the increase of visible light illumination time. A linear relation of $-\ln(C/C_0)$ vs reaction time was obtained, suggesting that the reaction can be considered as a pseudo-first-order reaction (Fig. 5b). The corresponding apparent kinetic rate constant (k) value of Co₂SnO₄-SnO₂/GC is estimated to be 0.017 min^{-1} , which is over 5.7 and 2.2 times higher than that of Co₂SnO₄ (0.003 min^{-1}) and Co₂SnO₄/SnO₂ (0.008 min^{-1}). Subsequently, the photocatalytic decomposing pathways for CTC were investigated by MS. From the mass spectra, the main m/z peaks located at 444, 362, 318, 274, 246, 194, 177, 167, 163, 148, 135, 121, 102, 92, and 74 were observed (Fig. 6a). The main intermediate with m/z value of 444 corresponds to CTC ($m/z = 515$) with the loss of one hydrochloric species and one chloridion. This can be further mineralized into m/z values of 362, which followed via the cleavage of C-N(CH₃)₂ forming intermediate with m/z values of 318. Then the byproducts could be degraded into possible intermediates with m/z values of 163, 167, 247 and 274 through the carboxylation, ring-opening reaction and so on. Subsequently, the intermediates were further oxidized into 2-methylbenzoic acid, benzoic acid, methyl acetate other molecules. According to the intermediates identified, the proposed degradation intermediates and reaction pathways of CTC were exhibited Fig. 6b. Moreover, the mineralization degree of CTC was examined by TOC analyzer during the degradation process. The TOC removal ratio gradually increased with the irradiation time was prolonged. The maximum TOC removal of CTC reached 76.39% after 80 min.

Additionally, the photocatalytic activity was also investigated for TC. As we anticipated, comparing with pure Co₂SnO₄ and Co₂SnO₄-SnO₂, Co₂SnO₄-SnO₂/GC also exhibited a superior degradation effect for TC once the reaction system was exposed to visible light irradiation (Fig. 5c). The removal efficiency achieved nearly 80% after 80 min.



Scheme 2. Schematic of the mechanisms for the different reactions over the Co_2SnO_4 - SnO_2 /GC heterojunction.

3.2.2. Catalytic reduction activity

The typical catalytic reaction of chemical reduction of *p*-NP by NaBH_4 was chosen to further evaluate the catalytic property of Co_2SnO_4 - SnO_2 /GC. As shown in Fig. 7a, the Co_2SnO_4 - SnO_2 /GC also exhibited more prominent catalytic performance compared with Co_2SnO_4 and Co_2SnO_4 / SnO_2 . The adsorption peak of *p*-NP solution around at 400 nm gradually dropped in intensity after adding of the catalyst with the proceeding of the reduction reaction, accompanying a new peak around at 300 nm due to the conversion of *p*-NP into *p*-AP (inset of Fig. 7a) [57]. The degree of the reduction was also presented by the ratio of C/C_0 . Complete conversion of *p*-NP to *p*-AP is obtained about 10 min. As Fig. 7b displayed, the reduction over Co_2SnO_4 - SnO_2 /GC composite follows the pseudo first-order kinetics. The k value was estimated to be 0.351 min^{-1} , which is over 3.1 and 2.3 times higher than that of Co_2SnO_4 (0.115 min^{-1}) and Co_2SnO_4 / SnO_2 (0.155 min^{-1}). The experimental results can well explain the excellent activity of Co_2SnO_4 - SnO_2 /GC composite for the reduction of *p*-NP with NaBH_4 .

3.3. Stability

Additionally, the stability of the catalysts was evaluated via a cycle experiment using Co_2SnO_4 - SnO_2 /GC composite. For each recycling test, Co_2SnO_4 - SnO_2 /GC was collected by centrifugation, and then washed with deionized water and ethanol for three times, respectively. As displayed in Fig. 8a, it is found that the catalytic performance of Co_2SnO_4 - SnO_2 /GC is hardly variation after testing more than four

times. As shown in Fig. 8b, the XRD analyses of the Co_2SnO_4 - SnO_2 /GC hybrid material were carried out before and after the catalytic reactions. Clearly, the main XRD peaks of the recycled Co_2SnO_4 - SnO_2 /GC have no obvious change. Therefore, the as-prepared Co_2SnO_4 - SnO_2 /GC hybrid material can be considered to be a stable and efficient catalyst.

3.4. Potential mechanism

The mechanism of GC to inhibit the recombination rate of photoinduced electron-hole pairs can be illustrated by the energy band-gap model of Scheme 2a. Co_2SnO_4 possess a narrow band gap (1.75 eV, Fig. 4b), hence under visible light irradiation, the electrons in the E_{VB} of Co_2SnO_4 would be excited into the conduction band and then injected into the more positive E_{CB} of SnO_2 , therefore, the photogenerated electrons and holes of Co_2SnO_4 can be separated effectively by the n-n junctions formed between the n-type Co_2SnO_4 and n-type SnO_2 interface, and the recombination of electron-hole pairs can be substantially retarded. It is well known that the good conductivity of GC promises fast electronic transmission between the semiconductors and GC. Hence, the electrons on E_{CB} of SnO_2 can be quickly transferred to GC instead of remain in SnO_2 lattice, which further facilitates charges separation in SnO_2 , which can lower the recombination of photoinduced and enhance the reaction rate in the photocatalytic process. Subsequently, residual holes within the Co_2SnO_4 E_{VB} may directly photooxidize CTC/TC. This conclusion was also supported by the active species trapping experiments (inset of Scheme 2a). Photooxidation by holes appears the primary pathway for CTC/TC degradation. It should be pointed out that the appearance of the special featured GC tends to facilitate the photocatalytic process. Furthermore, the highest photoactivity of Co_2SnO_4 - SnO_2 /GC could be derived from the synergistic effect, including the porous structure, high light absorbance and the favorable heterojunction structure.

On the other hand, the plausible mechanism for the reduction of *p*-NP is proposed (Scheme 2b). When Co_2SnO_4 - SnO_2 /GC was added into the mixed solution of *p*-NP and NaBH_4 , the BH_4^- and *p*-NP ions were easy adsorbed on the surface of Co_2SnO_4 - SnO_2 /GC. Subsequently, the NaBH_4 as an electron donor reacts with the Co_2SnO_4 component in the hybrid and transfers surface hydrogen species and electrons to them, and then flow to *p*-NP. Therefore, the catalysts act as a medium to transfer electrons from BH_4^- to *p*-NP resulting in the formation of *p*-AP [58,59]. The multiple intimate interfaces of Co_2SnO_4 - SnO_2 -GC assure rapid transmission of electrons; furthermore, the suitable GC coating increases of the adsorption capability for contaminant. Meanwhile, the cube hollow structure provides sufficient active sites, which is very favorable for the catalytic reaction [60]. That is, there exists a beneficial effect of coating Co_2SnO_4 - SnO_2 by GC and their synergistic effects in the Co_2SnO_4 - SnO_2 /GC hybrid.

4. Conclusions

In summary, Co_2SnO_4 - SnO_2 were successfully prepared via calcining $\text{CoSn}(\text{OH})_6$ and then subsequently used in the construction of Co_2SnO_4 - SnO_2 /GC composites with graphene-coated. Co_2SnO_4 - SnO_2 /GC heterojunctions were designed as a highly efficient multifunctional catalyst for photocatalytic and catalytic reduction reaction exhibited superior catalytic activity and high catalytic efficiency, which could be attributed to in situ generated SnO_2 , which increases the transfer interfaces (Co_2SnO_4 - SnO_2 -GC). Moreover, the synergistic effect of 2D GC nanosheets, which provides abundant exposed adsorption and reaction sites, high catalytic surface area and excellent electron shuttling from excited semiconductor to reaction sites which facilitates the charge transfer across Co_2SnO_4 - SnO_2 -GC heterojunction to catalytic reaction, the enhanced structural stability and reusability may also be due to the GC protective layer for Co_2SnO_4 - SnO_2 . This synthetic conception presents a new effective approach to prepare multifunctional catalysts to achieve environmental remediation.

Acknowledgements

This work was financially supported by the National Nature Science Foundation of China (No. NSFC51672116).

References

- [1] A. Molinari, E. Sarti, N. Marchetti, L. Pasti, *Appl. Catal. B: Environ.* 203 (2017) 9–17.
- [2] Z. Dong, X. Le, C. Dong, W. Zhang, X. Li, J. Ma, *Appl. Catal. B: Environ.* 162 (2015) 372–380.
- [3] T.R. Mandilimath, B. Gopal, *J. Mol. Catal. A: Chem.* 350 (2011) 9–15.
- [4] Y. Fan, W. Ma, D. Han, S. Gan, X. Dong, L. Niu, *Adv. Mater.* 27 (2015) 3767–3773.
- [5] C. Chen, W. Ma, J. Zhao, *ChemInform* 42 (2011) 4206–4219.
- [6] A. Bera, A.D. Sheikh, M.A. Haque, R. Bose, E. Alarousu, O.F. Mohammed, T. Wu, *ACS Appl. Mater. Interfaces* 7 (2015) 28404–28411.
- [7] M.B. Ali, F. Barka-Bouafel, H. Elhouichet, B. Sieber, A. Addad, L. Boussekey, M. Férid, R. Boukherroub, *J. Colloid Interface Sci.* 457 (2015) 360–369.
- [8] H. Zhang, F. Ke, Y. Li, L. Wang, C. Liu, Y. Zeng, M. Yao, Y. Han, Y. Ma, C. Gao, *Sci. Rep.* 5 (2015) 14417.
- [9] S.S. Mali, S.S. Chang, K.H. Chang, *Sci. Rep.* 5 (2015) 11424.
- [10] S.S. Shin, W.S. Yang, J.H. Noh, J.H. Suk, N.J. Jeon, J.H. Park, S.K. Ju, W.M. Seong, I.S. Sang, *Nat. Commun.* 6 (2015) 7410.
- [11] B.S. Joo, Y.J. Chang, L. Moreschini, A. Bostwick, E. Rotenberg, M. Han, *Curr. Appl. Phys.* 17 (2017).
- [12] S.S. Shin, E.J. Yeom, W.S. Yang, S. Hur, M.G. Kim, J. Im, J. Seo, J.H. Noh, S.I. Seok, *Science* 356 (2017) 167–171.
- [13] N. Rajamanickam, P. Soundarrajan, V.K. Vendra, J.B. Jasinski, M.K. Sunkara, K. Ramachandran, *Phys. Chem. Chem. Phys.* 18 (2016) 8468–8478.
- [14] L. Zhu, Z. Shao, J. Ye, X. Zhang, X. Pan, S. Dai, *Chem. Commun.* 52 (2015) 970–973.
- [15] A. Marikutsa, M. Rumyantseva, A. Baranchikov, A. Gaskov, *Materials* 8 (2015) 6437–6454.
- [16] D. Liu, S. Ren, X. Ma, C. Liu, L. Wu, W. Li, J. Zhang, L. Feng, *RSC Adv.* 7 (2017) 8295–8302.
- [17] M.B. Ali, A. Barras, A. Addad, B. Sieber, H. Elhouichet, M. Férid, S. Szunerits, R. Boukherroub, *Phys. Chem. Chem. Phys.* 19 (2017) 6569–6578.
- [18] M.B. Ali, A. Hamdi, H. Elhouichet, B. Sieber, A. Addad, Y. Coffinier, L. Boussekey, M. Férid, S. Szunerits, R. Boukherroub, *RSC Adv.* 6 (2017).
- [19] A.M. Ben, H.H. Yolcu, H. Elhouichet, B. Sieber, A. Addad, L. Boussekey, M. Moreau, M. Férid, S. Szunerits, R. Boukherroub, *J. Colloid Interface Sci.* 473 (2016) 66–77.
- [20] L. Li, L. Gu, L. Zheng, Z. Fan, G. Shen, *ACS Nano* 11 (2017) 4067–4076.
- [21] Y.J. Hong, Y.C. Kang, *Nanoscale* 7 (2015) 701.
- [22] R. Zhang, Y. He, A. Li, L. Xu, *Nanoscale* 6 (2014) 14221–14226.
- [23] G. Wang, Z.Y. Liu, P. Liu, *Electrochim. Acta* 56 (2011) 9515–9519.
- [24] B. An, Q. Ru, S. Hu, X. Song, J. Li, *Mater. Res. Bull.* 60 (2014) 640–647.
- [25] Z. Wang, Z. Wang, W. Liu, W. Xiao, X.W. Lou, *Energy Environ. Sci.* 6 (2012) 87–91.
- [26] G. Wang, X.P. Gao, P.W. Shen, *J. Power Sources* 192 (2009) 719–723.
- [27] H. Bouchaaba, B. Bellal, R. Maachi, M. Trari, N. Nasrallah, A. Mellah, *J. Taiwan Inst. Chem. Eng.* 58 (2016) 310–317.
- [28] H. Wang, L. Zhang, Z. Chen, J. Hu, S. Li, Z. Wang, J. Liu, X. Wang, *Chem. Soc. Rev.* 43 (2014) 5234–5244.
- [29] A. Shamirian, M. Edrisi, M. Naderi, *J. Mater. Eng. Perform.* 22 (2013) 306–311.
- [30] L. Yang, J. Huang, L. Shi, L. Cao, W. Zhou, K. Chang, X. Meng, G. Liu, Y. Jie, J. Ye, *Nano Energy* 36 (2017).
- [31] X.J. Wen, C.G. Niu, L. Zhang, G. Zeng, *ACS Sustai. Chem. Eng.* 5 (2017).
- [32] L. Jing, Y. Xu, S. Huang, M. Xie, M. He, H. Xu, H. Li, Q. Zhang, *Appl. Catal. B: Environ.* 199 (2016) 11–22.
- [33] X. Yang, F. Qian, G. Zou, M. Li, J. Lu, Y. Li, M. Bao, *Appl. Catal. B: Environ.* 193 (2016) 22–35.
- [34] S. Kumar, A. Baruah, S. Tonda, B. Kumar, V. Shanker, B. Sreedhar, *Nanoscale* 6 (2014) 4830.
- [35] J.A. Aguilar-Martínez, M.I. Pech-Canul, M. Esneider, A. Toxqui, S. Shaji, *Mater. Lett.* 78 (2012) 28–31.
- [36] C. Ma, W. Zhang, Y.S. He, Q. Gong, H. Che, Z.F. Ma, *Nanoscale* 8 (2016) 4121.
- [37] J. Wang, H. Li, S. Meng, L. Zhang, X. Fu, S. Chen, *Appl. Catal. B: Environ.* 200 (2016) 19–30.
- [38] A. Zhao, J. Masa, W. Xia, A. Maljusch, M. Willinger, G. Clavel, K. Xie, R. Schlögl, W. Schuhmann, M. Muhler, *J. Am. Chem. Soc.* 136 (2014) 7551–7554.
- [39] W. Kang, Y. Tang, W. Li, Z. Li, X. Yang, J. Xu, C.S. Lee, *Nanoscale* 6 (2014) 6551.
- [40] Z.Q. Liu, H. Cheng, N. Li, T.Y. Ma, Y.Z. Su, *Adv. Mater.* 28 (2016).
- [41] F. Song, H. Su, J. Chen, W.J. Moon, W.M. Lau, D. Zhang, J. Mater. Chem. 22 (2011) 1121–1126.
- [42] S. Joshi, S.J. Ippolito, M.V. Sunkara, *RSC Adv.* 6 (2016).
- [43] Y.D. Wang, C.L. Ma, X.D. Sun, *Nanotechnology* 13 (2002) 565.
- [44] Y. Chen, F. Sun, Z. Huang, H. Chen, Z. Zhuang, Z. Pan, J. Long, F. Gu, *Appl. Catal. B: Environ.* 215 (2017) 8–17.
- [45] S. Yuvaraj, S. Amareesh, Y.S. Lee, R.K. Selvan, *RSC Adv.* 4 (2014) 6407–6416.
- [46] L. Su, Y. Xu, J. Xie, L. Wang, Y. Wang, *ACS Appl. Mater. Interfaces* 8 (2016) 35172–35179.
- [47] J. Yin, Y. Li, F. Lv, M. Lu, K. Sun, W. Wang, L. Wang, F. Cheng, Y. Li, P. Xi, *Adv. Mater.* (2017) 29.
- [48] F. Lei, Y. Sun, K. Liu, S. Gao, L. Liang, B. Pan, Y. Xie, *J. Am. Chem. Soc.* 136 (2014) 6826–6829.
- [49] J. Bao, X. Zhang, B. Fan, J. Zhang, M. Zhou, W. Yang, X. Hu, H. Wang, B. Pan, Y. Xie, *Angew. Chem.* 54 (2015) 7399–74404.
- [50] R. Shi, Z. Li, H. Yu, L. Shang, C. Zhou, W. Gin, L.Z. Wu, T. Zhang, *ChemSusChem* 10 (2017) 4650–4656.
- [51] A. Akhundi, A. Habibiyangjeh, *Mater. Express* 5 (2015).
- [52] W. Zou, Y. Shao, Y. Pu, Y. Luo, J. Sun, K. Ma, C. Tang, F. Gao, L. Dong, *Appl. Catal. B: Environ.* 218 (2017) 51–59.
- [53] F. Chen, Q. Yang, X. Li, G. Zeng, D. Wang, C. Niu, J. Zhao, H. An, T. Xie, Y. Deng, *Appl. Catal. B: Environ.* 200 (2017) 330–342.
- [54] S. Yang, Y. Gong, J. Zhang, L. Zhan, L. Ma, Z. Fang, R. Vajtai, X. Wang, P.M. Ajayan, *Adv. Mater.* 25 (2013) 2452–2456.
- [55] J. Yang, D. Chen, Y. Zhu, Y. Zhang, Y. Zhu, *Appl. Catal. B: Environ.* 205 (2016).
- [56] H. Huang, K. Xiao, T. Zhang, F. Dong, Y. Zhang, *Appl. Catal. B: Environ.* 203 (2017) 879–888.
- [57] F. Wang, S. Song, K. Li, J. Li, J. Pan, S. Yao, X. Ge, J. Feng, X. Wang, H. Zhang, *Adv. Mater.* 28 (2016) 10679–10683.
- [58] C. Huang, W. Ye, Q. Liu, X. Qiu, *ACS Appl. Mater. Interfaces* 6 (2014) 14469–14476.
- [59] Y. Guo, L. Zhang, X. LIU, B. Li, D. Tang, W. Liu, W. Qin, J. Mater. Chem. A 4 (2016) 4044–4055.
- [60] J. Wang, A. Tang, L. Tan, H. Yang, J. Ouyang, *CrystEngComm* 19 (2017) 4824–4831.